KONA Powder and Particle Journal No. 31 (2014) 146–155/Doi:10.14356/kona.2014004 Original Research Paper

Characterization of Oxide-Dispersion-Strengthened (ODS) Alloy Powders Processed by Mechano-Chemical-Bonding (MCB) and Balling Milling (BM)†

Longzhou Ma[1]*, Bruce S.-J. Kang[2], Mary A. Alvin[3] and C. C. Huang[4]

[1] *Harry Reid Center for Environmental Studies, University of Nevada, USA*
[2] *Department of Mechanical and Aerospace Engineering, West Virginia University, USA*
[3] *US DOE National Energy Technology Laboratory, USA*
[4] *Hosokawa Micron Powder Systems, USA*

Abstract

Two types of powder processing techniques, Mechano-Chemical-Bonding (MCB) and MCB plus ball- milling (BM) with reduced time, have been employed to process the nickel-based oxide-dispersion-strengthened (ODS) alloy powders with composition of Ni-20Cr-5A1-3W-1.5Y_2O_3 to explore the alternate routes for fabricating, homogenizing and mechanical alloying (MA) the ODS alloy powders, which are usually processed by a prolonged ball-milling or rod-milling technique. In order to examine and evaluate the microstructure, morphology, blending homogeneity and MA effect of alloying powders, the commercial ball-milled ODS MA 956 alloy powders and experimental alloy powders processed by MCB only and MCB plus BM were subjected to microscopic and spectroscopic characterization and analysis using X-ray diffraction (XRD), scanning electron microscopy (SEM), and transmission electron microscopy (TEM). A FIB (focus ion beam) lift-out technique was employed to prepare the TEM cross-section samples of processed powders. The results showed that the MCB plus BM with reduced time could produce the ODS alloying powders with homogeneous lamellate structure similar to MA 956 powders processed by conventional BM technique with a prolonged period of time. The ODS alloy powders processed by MCB plus BM are to be utilized to fabricate the bulk ODS alloy product in the further research phase.

Keywords: oxide-dispersion-strengthened (ODS) alloy, Mechano-Chemical-Bonding (MCB), ball-milling (BM), X-ray diffraction (XRD), scanning electron microscopy (SEM), transmission electron microscopy (TEM), lamellate structure

1. Introduction

Nickel-based oxide-dispersion-strengthened (ODS) superalloys such as MA 956 or MA 6000, synthesized via mechanical alloying (MA) and consolidation process, exhibit the intermediate temperature strength as well as elevated temperature strength and creep resistance by means of the combined strengthening of gamma prime precipitates and nano-sized yttrium oxide (Y_2O_3) particles (Chou and Bhadeshia, 1993; Haghi and Anand, 1990; Howson et al., 1980). The Ni-based ODS superalloys are very promising for use in aircraft and advanced gas turbine engines due to their mechanical property and environmental resistance at high temperature. Also since yttria particles serve for interfacial pinning of the moving dislocations as well as yttria can be transformed to the nano-sized cluster during manufacturing, ODS alloys offer not only the improved creep resistance at elevated temperatures (up to 1200°C) but also low void swelling at condition of high energy high speed neutron irradiation. For example, recent extensively studied ferritic ODS alloys, MA 957 and 14WYT alloy with nominal composition of Fe-14Cr-1Ti-0.3Mo-0.3Y_2O_3 and Fe-14Cr-1Ti-3W-0.3Y_2O_3, respectively, are being considered for a number of advanced nuclear reactor applications at temperature of 500–600°C as well as in neutron irradiation higher than 300 dpa and elevated gas (Helium) concentration level owing to their high temperature strength and low void swelling (Odette et al., 2008; Schaublin et al., 2006; Ukai et al., 1998). Fabrication of ODS alloys is a complicated, costly and time-consuming process, which involves the

† Accepted: June 1, 2013
[1] Las Vegas, Box 454009, 4505 Maryland Parkway, Las Vegas, NV89154, USA
[2] Morgantown, WV26506, USA
[3] Pittsburgh, PA15236, USA
[4] Summit, NJ07901, USA
* Corresponding author:
E-mail: lma@nanosteelco.com
TEL: +1-702-217-2966 FAX: +1-208-552-2923

mechanical alloying (MA) powder metallurgical process, consolidation by hot deformation and post heat treatment (Gilman and Benjamin,1983; Suryanarayana, 2008). The MA process is the core step to fabricate ODS alloys, involving that the elemental alloying powders or oxide compounds are subjected to the high energy ball milling or rod milling for up to 60–72 hours to allow the nano-sized yttria particles to be dispersed homogenously throughout the master particles. After MA processing, the blended and alloyed powders are degassed, canned and consolidated by hot isostatic pressing (HIP) or hot extrusion. The consolidated material is then hot worked to semi-finished products. The hot worked material is further annealed and aged to yield the desired microstructure and properties for various applications. The complicated fabrication process has become a major barrier to commercially produce the ODS materials, leading to an extremely high raw material cost. For example, it costs about $345/kg for Ni-based ODS MA 956 alloy, however it only costs about $30–35/kg for Ni-based superalloys such as INCONEL 718 and 617 (Busby, 2009). In addition, numerous hours of MA milling time can cause high levels of contamination from milling debris and gaseous environment.

Recently developed Mechano-Chemical-Bonding (MCB) technology is an effective approach to blend alloying powders, forming the composite particles consisting of the hosting particles as core and small particles or fibres that are coated around the core. The MCB-induced particle bonding process takes place in the solid state without needing solvents or external heating avoiding potential contaminations and reactions. During MCB processing, the starting powder mixtures are subjected to high compression, shear, and impact forces as they pass through a narrow gap in a high speed rotating device. As a result, the particles are dispersed, mixed, shaped, and bonded together, consequently forming the composite particles composed of various combinations of the starting ingredients (Du Pasquier et al., 2009; Murata et al., 2004; Nam and Lee, 1999; Welham et al., 2000). So far, the green MCB technology has been utilized to make various composite particles used in the fields of functional gradient materials, batteries, cermets, fuel cells, polymers, cosmetics, and pharmaceuticals. Preliminary studies showed that utilization of MCB processing to blend ODS alloying powders was able to homogenously disperse yttrium oxides on the base particles to form the composite structure (Kang et al., 2010). Also, the newly developed MCB processing technique is simple, environmentally friendly, and can be scaled up to 300 litres per batch. Thus, MCB or its combination technique is considered as an enhancement or alternative to the conventional mechanical alloying (MA) process using balling milling or rod milling.

In this study, the technique of MCB as well as MCB plus BM with reduced time were employed to process the ODS alloying powders to explore the alternative method of the conventional time-consuming ball milling or rod milling technique. The processed alloying powders were examined and analyzed microscopically and spectroscopically using TEM, SEM and XRD to identify the mechanical alloying effects such as powder microstructure, morphology, and chemical homogeneity. In order to compare the blending effects, commercial ODS MA 956 alloy powders processed by conventional BM were examined in parallel as a benchmark, while it is iron-based. As a preliminary research phase, the goal of this study is to examine the mechanical alloying effects produced by the proposed techniques, MCB only and MCB plus BM. The processed ODS alloying powders will be either used as spray powders for advanced coating or followed by canning, HIP, hot rolling and annealing to form final ODS products in the next research phase. This study is an attempt to fabricate the ODS alloying powders using the proposed techniques as a substitute or to simplify and improve the MA processes.

2. Materials and Experiments

2.1 Materials

Commercial metallic and ceramic powders including Y_2O_3 (< 50 nm, 99.99% pure), Al (4.5–7 μm, 97.5% pure), Cr (7.5–10 μm, 99.5% pure), and Ni (4–8 μm, 99.9% pure) were purchased from Sigma Aldrich Inc. Saint Louis, MO., Alfa Aesar, Ward Hill, MA, F.W. Winter Inc. & Co. Camden, NJ, and Atlantic Equipment Engineers, Bergenfield, NJ, respectively. These powders were stored separately in an inert environment in sealed bottles full of argon gas. Considering the short time milling as well as no ball-powder-ball collision involved during MCB only process, the average sizes of all starting powder constituents ranged from 0.5 to 15 microns in this study (Du Pasquier et al., 2009; Nam and Lee, 1999; Welham et al., 2000). For conventional ball milling or rod milling MA process, however, the starting powders usually have average diameters ranging from 30 to 500 microns (Suryanarayana, 2008). The starting powders were initially mechanically blended under gas protection inside a glove box chamber according to the nominal composition (wt%) of Ni-20Cr-5Al-3W-1.5 Y_2O_3. The just-blended powders were then placed into bottles that were sealed and filled with argon gas to prevent oxidation of powders. Each bottle containing the just-blended ODS alloying powder sample weighed approximately 200 g. To compare the effects of different processing techniques, the commercial ODS MA 956 alloy powders, which have a nominal composition of Fe-20Cr-4.5Al-0.5 Y_2O_3-0.5 Ti and have been subjected to conventional BM at 200 RPM (rota-

tion per minute) for 72 hours, was obtained from Special Metals Co., Huntington, WV, as a benchmark material.

2.2 Powder Processing

Two types of processing technique, MCB only and MCB plus BM, were employed to process the as-just-blended starting powders to fabricate the experimental ODS alloy powders. For MCB only procedure, the starting powders were MCB processed at a speed to 4000 RPM for only 30 minutes. It was expected to have Y_2O_3 nanoparticles dispersed and bonded onto the surfaces of larger hosting particles such as Ni and Cr particles, which in turn created oxide dispersion and MA (mechanical alloying) effects. After MCB processing, the powders were stored in the sealed bottles filled with argon gas. The MCB processing was conducted in Hosokawa Micron Powder Systems, Summit, NJ. Following MCB processing, a portion of MCB-processed powders (200 g) was then conducted ball milling (BM) at 200 rpm for 20 hours under inertial gas protection condition. Considering the powders have been processed using high speed MCB for 30 minutes, the BM processing time was reduced to 20 hours in comparison with conventional BM time of 70 hours for MA processing. The BM processing was performed at West Virginia University, Morgantown, WV. After processing, small amount of powders (5–10 g) were taken for micro-structural analysis using TEM (transmission electron microscopy), SEM (scanning electron microscopy) and XRD (X-ray diffraction), and the rest of powders were stored for the next research phase use. The micro-structural analysis of experimental powders was conducted at University of Nevada Las Vegas, NV.

2.3 Characterization

2.3.1 X-Ray Diffraction (X-RD) Analysis

The processed powders were characterized by X-ray powder diffraction (XRD) using a PANalytical X'Pert PRO X-ray diffractometer with a CuKα radiation (45 kV, 40 mA), and a multiple-strip solid state detector (X'Celerator®). The sample was prepared by suspending 2–3 g powders in ethanol to make slurry. The slurry was then set on a low-background silicon sample holder. The XRD patterns were recorded at room temperature with step-sizes of 0.017°, 2θ, and 46 s per step. The phase constitution and crystallographic parameters were characterized using the International Center for Diffraction Database (ICDD) for powder diffraction data. The analysis of line broadening effect would be conducted to measure the mechanical deformation and crystal size.

2.3.2 Electron Microscopy (EM) Analysis

The microstructure, morphology, topology and elemental chemical distribution of the processed powder samples were studied by EM techniques including scanning electron microscopy (SEM) and transmission electron microscopy (TEM). SEM imaging was performed on a JEOL scanning electron microscope, JSM-5610 SEM, equipped with secondary electron (SE) and backscattered electron (BE) detectors and an Oxford ISIS EDS system. The acceleration voltage used in SEM was 15–18 kV using the SEM BE and SE mode. In order to improve the conductivity and image contrast, the powder samples were coated with a layer of gold. Gold-coated samples were suspended on the double-sided carbon tapes for SEM observation and imaging. Also, SEM images of processed powders were employed to measure the size of powder particle using an image processing software, Image J with version of 1.46. Note that since most particles showed round morphology, the particle size indeed referred to an equivalent diameter of a particle. Following the particle analysis procedure of Image J, 10 SEM images totally at least containing about 200 sampling particles were analysed to obtain the particle size at different processing conditions.

A TECNAI-G2-F30 transmission electron microscope with a 300 keV field emission gun was used to characterize the powder samples. Samples were analyzed using the conventional bright field (BF), selected-area diffraction (SAD) and high-angle annular dark-field scanning-transmission electron microscopy (HAADF-STEM) mode for defects, diffraction and Z-contrasting imaging, respectively. All TEM images were recorded using a Gatan SC 200 CCD camera with resolution of 2k × 2k. The elemental distribution of each sample was also determined using the corresponding X-ray energy dispersive spectrometry (EDX) under the STEM mode. For STEM/EDX mode, the electron probe with a size of 0.2 nm was used to examine the dedicated area of sample. In order to examine the internal microstructure of processed powders using TEM in a finer scale, the cross-sectioned TEM sample of experimental powders was prepared, involving that 4–6 mg of powders were mixed with spur resin in a micro-vial, which was then solidified by furnace drying at 60°C overnight. The spur resin used for these samples was a mixture of 10.0 g of ERL (vinylcyclohexene dioxide), 4.0 g of DER (a diglycidyl ether of polypropylene glycol), 26.0 g of NSA (nonenyl succinic anhydride), and 0.4 g of DMAE (dimethylaminoethanol). The powders embedded in the resin was then thinned into membranes with a thickness of 50–80 nm using a FEI Nova 200 FIB (focus ion beam) system, which combines the FIB technology with SEM in a single tool. This system can provide SEM imaging in order to monitor the whole process during FIB milling. A FIB cross-section lift-out technique based on a TEM-wizard program in FIB system was used to obtain the cross-sectioned TEM sample of powders (Giannuzzi and Stevie, 1999; Stevie et al.,

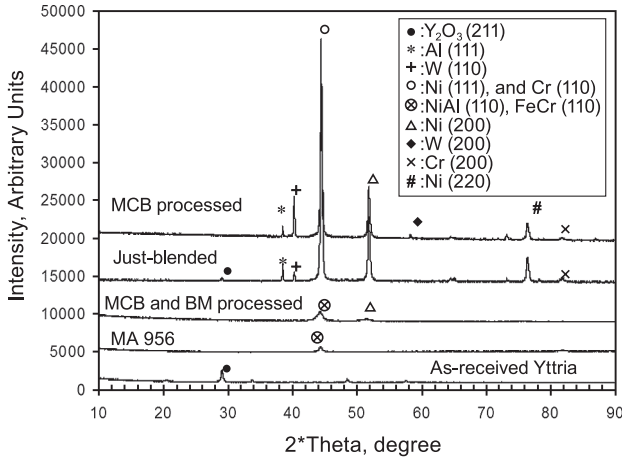

Fig. 1 XRD patterns of starting and processed powders.

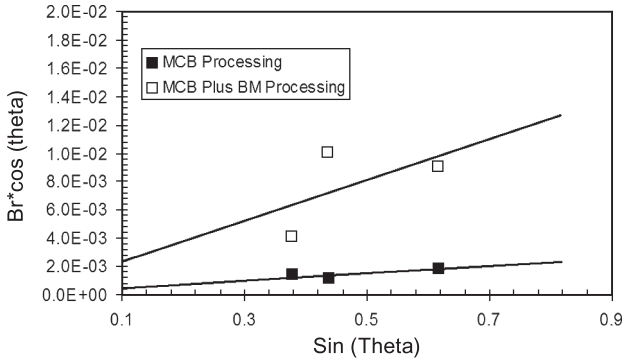

Fig. 2 Analysis of line-broadening effect.

2001). The preparation of TEM cross-sectioned samples by FIB was conducted at Arizona State University, Tempe, AZ.

3. Results and Discussions

3.1 X-RD Analysis

Fig. 1 presented the X-RD spectrum of all experimental powder samples including as-received Y_2O_3 powder, as-blended starting powder, MCB processed powder, MCB plus BM processed powder, and commercial MA 956 powder samples. For as-received yttria and just-blended starting powders, the typical sharp diffraction peaks of all alloying constituents, Al, Cr, Ni, W and Y_2O_3 were observed in X-RD spectrum. The spectrum of as-received Y_2O_3 particles displayed the line-broadening effects due to nano-scaled size of yttria. For MCB processed sample, all individual alloying elemental peaks are still observed with identical intensities relative to the spectrum of just-blended sample. Also the line broadening effect was noticed in spectrum of MCB processed sample, suggesting small deformation occurred during MCB processing. However, for MA 956 and MCB plus BM processed samples, only major elemental peaks with substantially reduced intensities, NiAl (110) and FeCr (110) peaks, were observed, suggesting significant change of crystallographic structure due to formation of solidified phase and presence of defects compared to the spectrum of as-blended sample. Also, extensive line-broadening effects were evident for MA 956 and MCB plus BM processed samples, suggesting extensive plastic deformation involved during processing. Using the peak width of just-blended powders as a reference, the line-broadening effect could be used to estimate the micro-strain and crystal size of powder. X-RD line broadening effect is usually contributed from micro-strain, fine crystal size, and systematic error of instrument. The following equation can be written to account for these contributions (Cullity and Stock, 2001; Suryanarayana and Norton, 1998):

$$B_r \cos\theta = \frac{k\lambda}{L} + \eta \sin\theta \tag{1}$$

Where, B_r is peak FWHM (full width at half maximum); θ is diffraction angle; k is a constant (0.89–1.39); λ is X-ray wavelength; L is the average crystal size; and η is micro-strain of crystal.

Using the average width at FWHM, B_r, and corresponding diffraction angle, θ, obtained from spectrum, **Fig. 2** presents $B_r \times \cos(\theta)$ as a function of $\sin(\theta)$ based on equation (1). The slop and intercept of the fitting line represent the micro-strain and crystal size of powder, respectively. From **Fig. 2**, the powders processed by MCB have micro-strain of 0.26% and crystal size of 720 nm, and the powders processed by MCB plus BM have micro-strain of 1.45% and crystal size of 177 nm. The X-RD broadening analysis suggests that MCB plus BM produced larger strain and smaller crystal size than MCB only. X-RD spectrum analysis of powders processed by MCB indicates that the MCB process in this study would not remarkably change the crystallographic structure and powder size, and MCB could disperse the nano-sized Y_2O_3 particle resulting in the disappearance of Y_2O_3 peak in XRD spectrum.

3.2 SEM Microscopy

SEM imaging was conducted on the experimental powder samples showing the morphology, topology, and dimension. **Fig. 3** presents SEM micrographs of MA 956 powders and experimental powders processed by MCB and MCB plus BM, indicating that conventional BM and MCB plus BM processing produced the random shaped particles, **Fig. 3 (a)** and **(b)**. The insets in **Fig. 3 (a)** and **(b)** show that the powders processed by BM and MCB plus BM contain numerous lamellate structures, suggesting that large deformation, cold-welding, and fracture

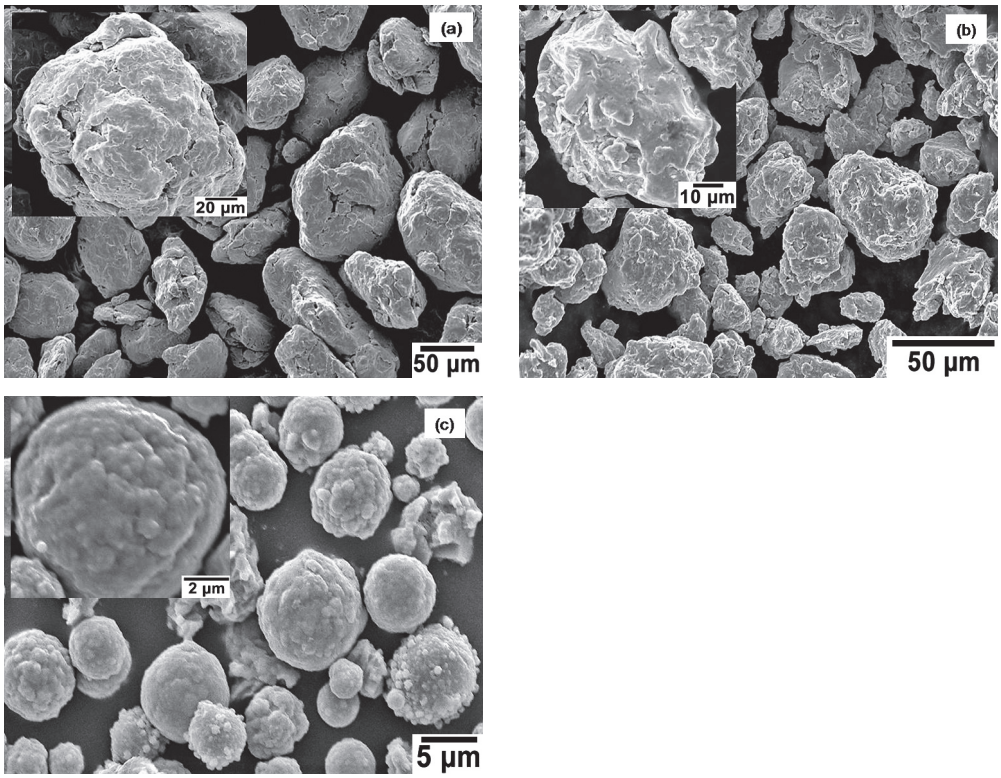

Fig. 3 SEM micrographs of processed powders. (**a**) Powders of MA 956, (**b**) Powders processed by MCB plus BM and (**c**) Powders processed by MCB only.

occurred during processing. For powders processed by MCB only, the powder size almost kept unchanged comparing to the starting size, **Fig. 3 (c)**. However the composite structure and topography was observed, indicating small particles were bonded with master particle forming the composite one as seen in insets. All MCB processed powders keep spherical, suggesting small crystal microstrain. Based on the SEM observation results, particle analysis of processed powders was conducted to statistically measure the distribution of effective particle size. **Fig. 4** plots histogram of particle size distribution for powders subjected to different processing, indicating that MA 956 alloy powders, powders processed MCB plus BM, and powders processed by MCB have mean effective particle size of 121.50, 28.42, and 5.40 μm, respectively.

3.3 TEM Microscopy and Spectroscopy

As an example, **Fig. 5** presents SEM micrographs of TEM cross-sectioned powder sample prepared by a FIB lift-out technique procedure for the powders processed by MCB, showing powder particles were mounted by the spur resin and particle area in resin specimen was delineated and protected from sputtering by deposition of a platinum line. Then, trenches were cut and milled in front and back of the deposited line until an electron-transparent membrane was available, **Fig. 5 (a)**. The thin membrane was cut at all ends, lift out by a needle, and welded on a grid for TEM observation, **Fig. 5 (b)** and **(c)**. **Fig. 6** presents TEM micrographs of the cross-sectioned powder sample of MA 956 alloy powders. TEM BF image in **Fig. 6 (a)** showed numerous of defects and lamellar structures, and inset with high magnification showed the lamellar structures contained lots of moiré fringes, indicating heavy deformation occurred during powder BM processing. The overall microstructure of MA 956 powder is very uniform. The corresponding SAD image in **Fig. 6 (b)** reflects the ring patterns with Fe, Cr and solid-solution phase (FeCr) contribution. The Fe-matrix produced diffuse rings, suggesting fine grains of heavily deformed. The FeCr phase was identified which was consistent with XRD results.

Fig. 7 and **Fig. 8** show TEM micrographs of samples processed by MCB plus BM and MCB, respectively. Compared to the well-defined lamellar structures of MA 956 alloy powders, TEM BF image of powder sample processed by MCB plus BM displays numerous deformed fragments and defects, **Fig. 7 (a)**. Some layered structures still appeared and inset shows numerous moiré fringes. **Fig. 7 (b)** represents the corresponding SAD pattern including Ni-matrix diffuse ring, faint rings and spots associated with reflections of Ni, Cr, NiCr, and yttria, suggesting formation of secondary phase, NiAl, and the presence of some un-deformed metals. For powder sample

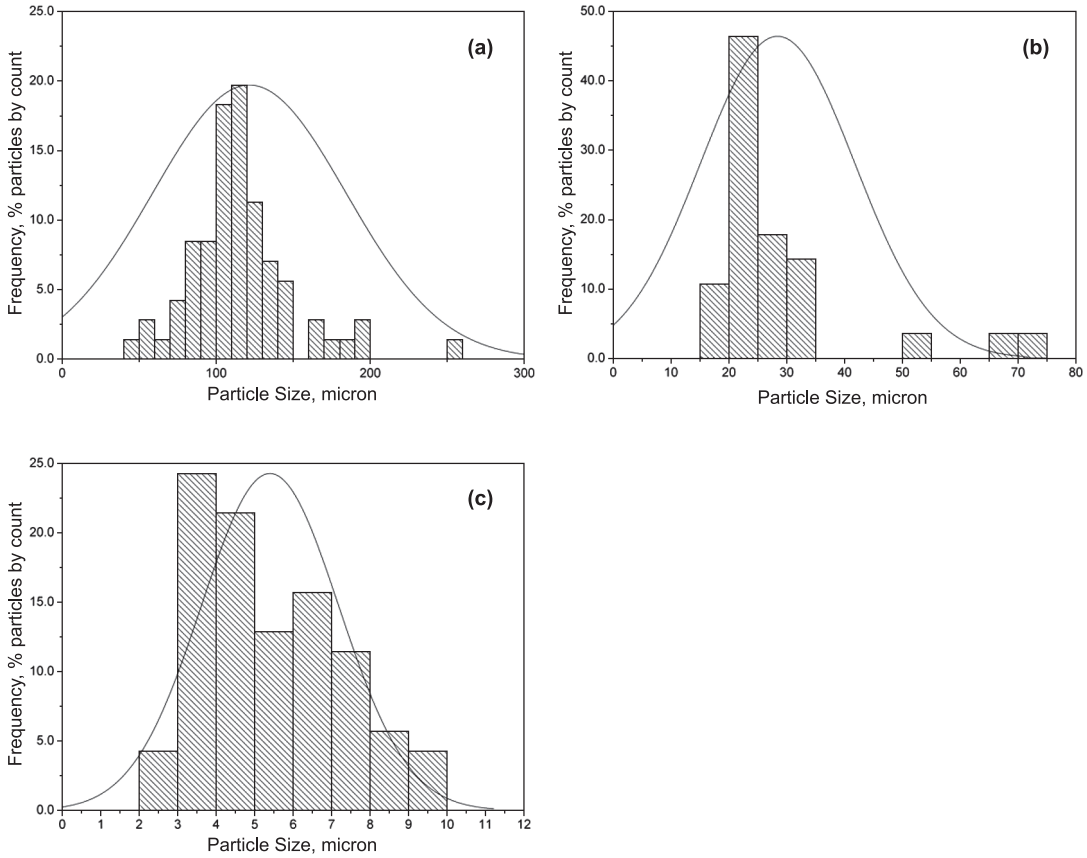

Fig. 4 Histogram of size distribution of processed powders. (**a**) Powders of MA 956, (**b**) Processed by MCB plus BM, and (**c**) Processed by MCB only.

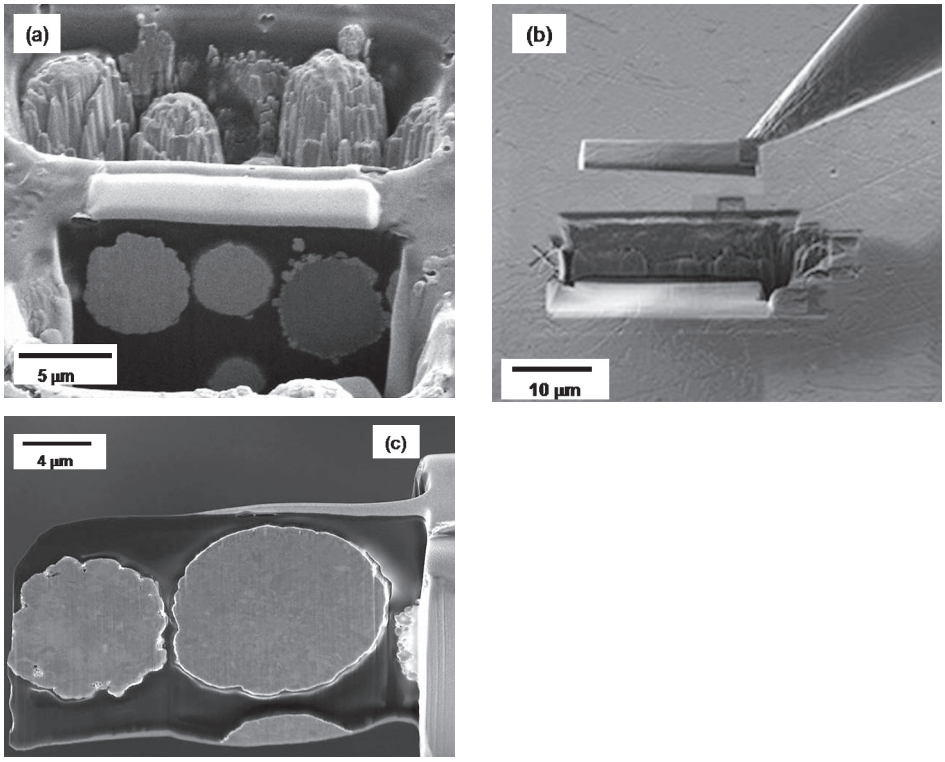

Fig. 5 Powder TEM cross-section sample preparation by FIB Lift-out procedure. (**a**) A metal line was deposited over region of interest and trenches were milled in the front and back side of deposited line. (**b**) A membrane was cut and picked out. (**c**) A TEM cross-section sample of powders processed by MCB.

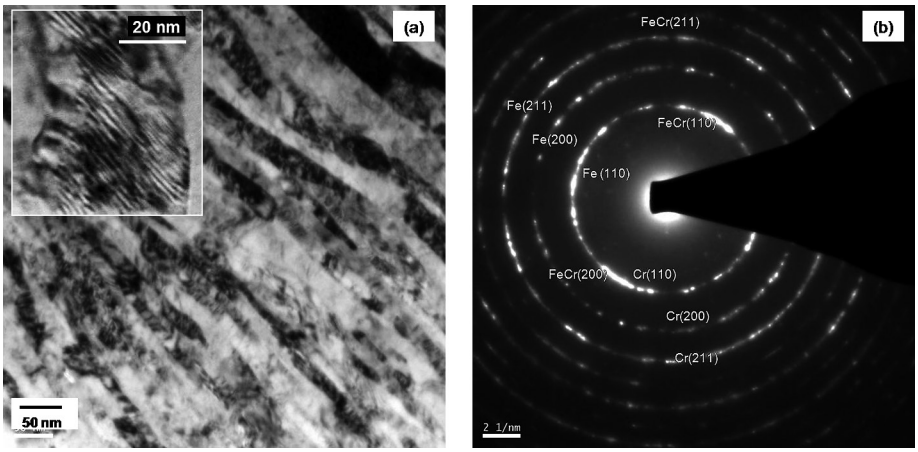

Fig. 6 TEM micrographs of MA 956 powder sample. (**a**) TEM BF image, (**b**) Corresponding SAD image.

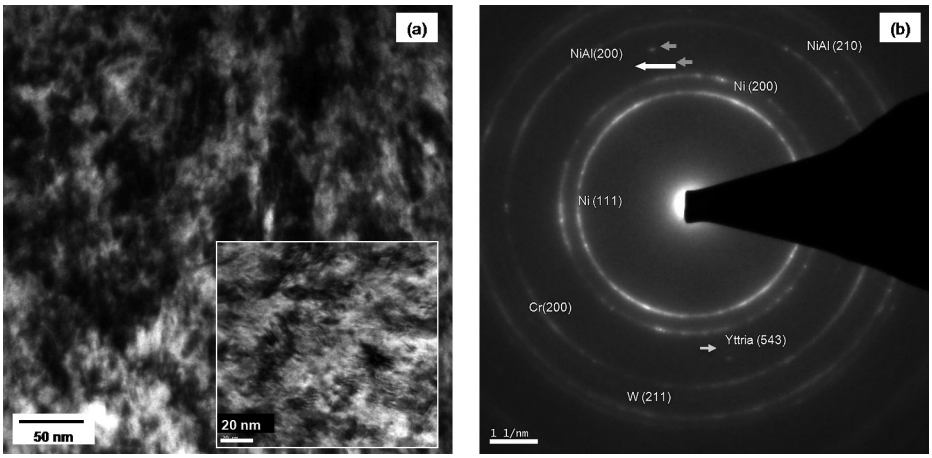

Fig. 7 TEM micrographs of powders processed by MCB plus BM. (**a**) TEM BF image, (**b**) Corresponding SAD image.

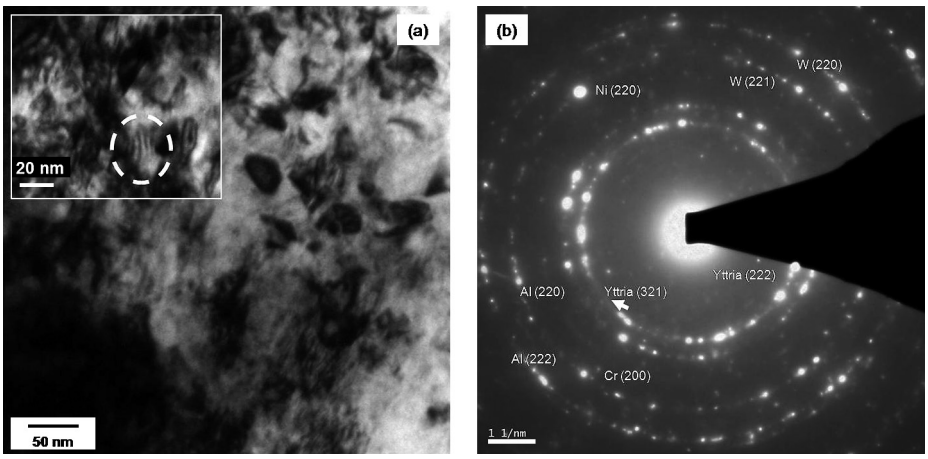

Fig. 8 TEM micrographs of powders processed by MCB. (**a**) TEM BF image, (**b**) Corresponding SAD image.

processed by MCB only, lamellar structure did not appear in TEM BF image, **Fig. 8 (a)**. Instead, lots of nano-sized particles distributed on the Ni-matrix and moiré fringes are still visible, but amount is less than samples processed by BM and MCB plus BM. SAD pattern in **Fig. 8 (b)** shows lots of individual spots associated with Ni, Al, Cr, and yttria reflection, indicating lots of metal particle were bonded with matrix, but solid-solution phase wasn't formed yet. Therefore, powders processed by MCB plus BM have similar microstructure to MA 956 powder, while

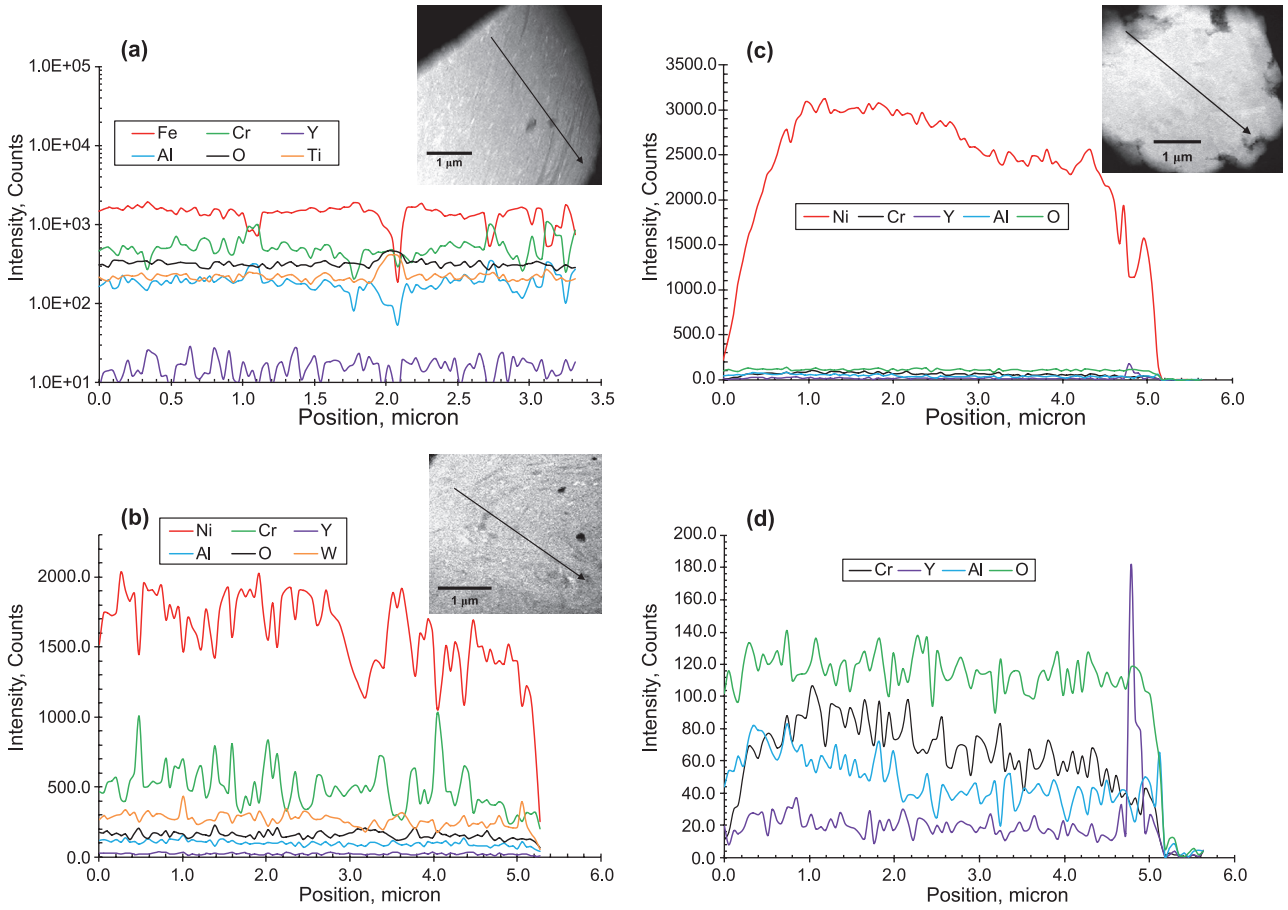

Fig. 9 STEM/EDX line-scanning analysis. (**a**) MA 956 powder sample, (**b**) MCB plus BM processed sample, (**c**) MCB processed powder sample, and (**d**) Close-viewed plot of (**c**).

the latter has more uniform lamellar structure. To get better MA and dispersion effects using MCB plus BM route, a proper combination of the starting powder sizes, energy input, and MCB processing time should be optimized.

In order to examine the chemical homogeneity of alloying elements across the powder cross-section, STEM Z-contrast imaging and EDX line-scanning analysis were conducted. **Fig. 9** presents the results of EDX line-scanning analysis and the insets show Z-contrast imaging and scanning direction. For MA 956 and MCB plus BM processed powder sample, EDX line scanning results show the alloy elements and Y_2O_3 have been dispersed homogeneously throughout the matrix, and Fe-Cr and Ni-Cr could be exchangeable, **Fig. 9 (a)** and **(b)**. The inset images show the homogeneous contrast profile, indicating the homogeneous distribution of elements. For powder sample processed by MCB as seen in **Fig. 9 (c)**, Ni-matrix particle displays strong intensity and other elements are relatively weak but detectable. **Fig. 9 (d)** was the close-view of EDX spectrum with weak counts in **Fig. 9 (c)**, indicating that yttrium was detected distributing around the edge of particle as highlighted by circle. Z-contrast image of hosting particle show deformation occurred around particle edge.

4. Conclusions

A Mechano-Chemical-Bonding (MCB) as well as MCB plus ball milling (BM) with reduced time technique was used to fabricate, blend and homogenize the oxide dispersion-strengthened (ODS) nickel-based superalloy powders. The processed powders and MA 956 alloy powders have been characterized using X-RD, SEM and TEM. The results suggested the following conclusions:

1. As a benchmark material, MA 956 alloy powders subjected to prolonged BM processing contained numerous uniform lamellar structures, moiré fringes, and defects. The solid solution phase, FeCr, has been formed during BM, and alloying elements have been homogeneously dispersed.

2. Utilization of MCB and MCB plus BM technique to blend the ODS alloying powders could introduce the lattice strain, and defects. The technical route of MCB plus BM generated larger strain and smaller crystal size than MCB.

3. The MCB processing could produce composite particles bonded with other small particles such as nano-sized yttria.

4. MCB plus BM with reduced time could produce the homogeneous lamellate structure and chemical homoge-

neity similar to MA 956 alloy powders. As an alternate, MCB plus BM process is possible to be employed to prepare ODS powders with reduction of BM time. Further exploring the effects of MCB plus BM processing parameters on microstructure and morphology of ODS alloying powders would be necessary to optimize the process. Also, follow-up work to produce surface coating or to fabricate ODS alloy final products by HIP, hot deformation and heat treatment using the MCB processed powders are necessary to validate this technical route.

5. MCB technique is potential to be employed to disperse only nano-sized yttria particles on the pre-alloyed micron-sized hosting particles to fabricate ODS alloying powders.

Acknowledgements

This research is supported by US Department of Energy, National Energy Technology Laboratory (NETL), and Advanced Research Materials (ARM) Program under RDS Contract DE-AC26-04NT41817.606.01.01. The encouragement and support by Patricia Rawls and Robert Romanosky, Program Managers, are very much appreciated. Thanks are also due to TRP (Transmutation Research Program), University of Nevada, Las Vegas, for supporting X-RD, SEM and TEM analysis in instrument usage and working time.

References

Busby J.T., Economic benefits of advanced materials in nuclear power systems, Journal of Nuclear Materials, 392 (2009) 301–306.

Chou T.S., Bhadeshia H.K.D.H., Crystallographic texture in mechanically alloyed oxide dispersion-strengthened ma956 and ma957 steels, Metallurgical Transactions A, 24 (1993) 773–779.

Cullity B.D., Stock S.R., Elements of X-Ray Diffraction, 3rd ed., Prentice—Hall, New Jersey, 2001, pp. 174–177.

Du Pasquier A., Huang C.C., Spitler T., Nano $Li_4Ti_5O_{12}$–2no $_2O_4$ batteries with high power capability and improved cycle-life, Journal of Power Sources, 186 (2009) 508–514.

Giannuzzi L.A., Stevie F.A., A review of focused ion beam milling techniques for tem specimen preparation, Micron, 30 (1999) 197–204.

Gilman P.S., Benjamin J.S., Mechanical alloying, Annual Review of Materials Science, 13 (1983) 279–300.

Haghi M., Anand L., High-temperature deformation mechanisms and constitutive equations for the oxide dispersion-strengthened superalloy ma 956, Metallurgical Transactions A, 21 (1990) 353–364.

Howson T.E., Mervyn D.A., Tien J.K., Creep and stress rupture of a mechanically alloyed oxide dispersion and precipitation strengthened nickel-base superalloy, Metallurgical Transactions A, 11 (1980) 1609–1616.

Kang B., Ogawa K., Ma L.-Z., Alvin M.A, Smith G., ODS coating development by cold spray method using powder mix prepared by combined MCB and ball milling processes, 24th Annual Conference on Fossil Energy Materials, Pittsburgh, PA, USA, May 25–27, 2010.

Murata K., Fukui T., Huang C.C., Naito M., Abe H., Nogi K., Composite powders processed by an advanced mechanical method for the fabrication of cermet anodes of solid oxide fuel cells, Journal of Chemical Engineering of Japan, 37 (2004) 568–571.

Nam J.G., Lee J.S., Mechano-chemical synthesis of nanosized stainless steel powder, Nanostructured Materials, 12 (1999) 475–478.

Odette G.R., Alinger M.J., Wirth B.D., Recent developments in irradiation-resistant steels, Annual Review of Materials Research, 38 (2008) 471–503.

Schäublin R., Ramar A., Baluc N., De Castro V., Monge M.A., Leguey T., Schmid N., Bonjour C., Microstructural development under irradiation in european ods ferritic/martensitic steels, Journal of Nuclear Materials, 351 (2006) 247–260.

Stevie F.A., Vartuli C.B., Giannuzzi L.A., Shofner T.L., Brown S.R., Rossie B., Hillion F., Mills R.H., Antonell M., Irwin R.B., Purcell B.M., Application of focused ion beam lift-out specimen preparation to tem, sem, stem, aes and sims analysis, Surface and Interface Analysis, 31 (2001) 345–351.

Suryanarayana C., Recent developments in mechanical alloying, Reviews on Advanced Materials Science, 18 (2008) 203–211.

Suryanarayana C., Norton M.G., X-Ray Diffraction: A Practical Approach, Plenum Press, New York, 1998. pp. 207–221.

Ukai S., Nishida T., Okuda T., Yoshitake T., R&d of oxide dispersion strengthened ferritic martensitic steels for fbr, Journal of Nuclear Materials, 258–263, Part 2 (1998) 1745–1749.

Welham N.J., Willis P.E., Kerr T., Mechanochemical formation of metal–ceramic composites, Journal of the American Ceramic Society, 83 (2000) 33–40.

Author's short biography

Longzhou Ma

Dr. Longzhou Ma is formerly a research scientist of Materials Engineering at Harry Reid Center for Environmental Studies, University of Nevada Las Vegas. Currently, Dr. Longzhou Ma is a senior research engineer of R & D, NanoSteel Company, Inc., Idaho Falls, ID83404. His expertise includes microstructure characterization using transmission electron microscopy (TEM), scanning electron microscopy (SEM), optical microscopy. Dr. Ma is also known for his expertise in dislocation analysis in materials structure and crack propagation analysis in metallic materials. Over the years, he has published over 35 peer-reviewed papers. Dr. Ma has affiliation with numerous engineering society including TMS, MRS, MSA. As a PI or co-PI, he ever involved several US DOE-sponsored research projects. Dr. Ma can be reached at lma@nanosteelco.com.

Bruce S.-J. Kang

Dr. Bruce Kang is a Professor at the Mechanical and Aerospace Engineering Department, West Virginia University. Dr. Kang's current research activities include: (1) SOFC and CO2 re-use, (ii) Biomass energy conversion, (iii) high temperature materials for advanced power systems, (iv) experimental and multi-scale computational modeling analyses of metallic and intermetallic alloys, and (vi) surface material property evaluation using micro/nano indentation.

Mary A. Alvin

Mary Anne Alvin, DOE NETL: Ms. Alvin currently serves as a Division Director for the Office of Research and Development (ORD), Department of Energy's National Energy Technology Laboratory. She also leads ORD's advanced gas turbine engine materials development and heat transfer research efforts for land-based power generation. Prior to joining DOE NETL in 2005, Ms. Alvin had thirty years of experience at Westinghouse and Siemens Westinghouse, working in the area of advanced energy system. Ms. Alvin was awarded the Siemens Westinghouse Eagle Award in 1999, which is the highest corporate award at Siemens that is granted to an employee. She currently holds twenty-six patents with additional pending.

C. C. Huang

Dr. C. C. Huang is the Director of Business & Technology Development at Hosokawa Micron Powder Systems, an operating unit of Hosokawa Micron International Inc., a global supplier of systems and equipment related to material sciences and engineering. He holds an M.S. degree in engineering from Illinois Institute of Technology and a Ph.D. degree in chemical engineering from West Virginia University. Dr. Huang specializes in powder and nanoparticle processing, powder characterization, powder granulation, and fluidization. He has published over 30 articles and 8 patents, chaired several meetings, and is an active member in a number of scientific and engineering societies.